Environmental Science & Technology

Article

pubs.acs.org/est

Isotope-Based Source Apportionment of EC Aerosol Particles during Winter High-Pollution Events at the Zeppelin Observatory, Svalbard

Patrik Winiger,[†] August Andersson,[†] Karl E. Yttri,[‡] Peter Tunved,[†] and Örjan Gustafsson*,[†]

[†]Department of Environmental Science and Analytical Chemistry (ACES) and the Bolin Centre for Climate Research, Stockholm University, SE-106 91 Stockholm, Sweden

[‡]NILU - Norwegian Institute for Air Research, NO-2027 Kjeller, Norway

Supporting Information

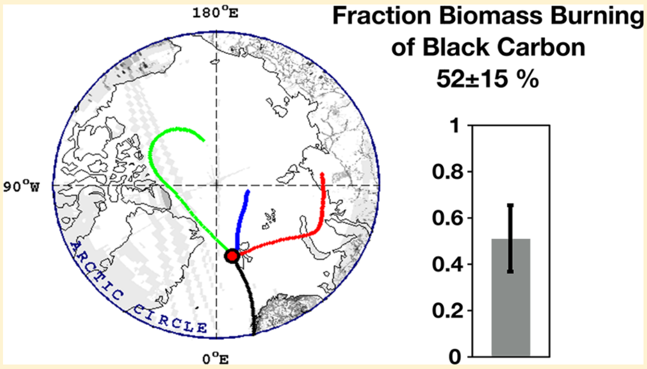

ABSTRACT: Black carbon (BC) aerosol particles contribute to climate warming of the Arctic, yet both the sources and the source-related effects are currently poorly constrained. Bottom-up emission inventory (EI) approaches are challenged for BC in general and the Arctic in particular. For example, estimates from three different EI models on the fractional contribution to BC from biomass burning (north of 60° N) vary between 11% and 68%, each acknowledging large uncertainties. Here we present the first dual-carbon isotope-based ($\Delta^{14}C$ and $\delta^{13}C$) source apportionment of elemental carbon (EC), the mass-based correspondent to optically defined BC, in the Arctic atmosphere. It targeted 14 high-loading and high-pollution events during January through March of 2009 at the Zeppelin Observatory (79° N; Svalbard, Norway), with these representing one-third of the total sampling period that was yet responsible for three-quarters of the total EC loading. The top-down source-diagnostic ^{14}C fingerprint constrained that 52 ± 15% (n = 12) of the EC stemmed from biomass burning. Including also two samples with 95% and 98% biomass contribution yield 57 ± 21% of EC from biomass burning. Significant variability in the stable carbon isotope signature indicated temporally shifting emissions between different fossil sources, likely including liquid fossil and gas flaring. Improved source constraints of Arctic BC both aids better understanding of effects and guides policy actions to mitigate emissions.

INTRODUCTION

Light-absorbing black carbon (BC) aerosol particles contribute to the ongoing warming of the Arctic.[1] Recent estimates suggest that the globally averaged radiative forcing of BC is second only to CO_2, but the uncertainties for BC are much larger.[1−3] In winter and early spring, levels of air pollutants, including BC, are enhanced in the Arctic troposphere, giving rise to a phenomenon referred to as "Arctic Haze".[4−6] Long-term observational records of BC in the Arctic are scarce and scattered, and current atmospheric chemistry-transport and climate models both underestimate the loadings of BC and fail to reproduce much of the observed seasonality of Arctic BC concentrations.[7,8]

BC forms through the incomplete combustion of biomass (e.g., residential wood burning and wildfires) and fossil fuels (e.g., traffic, coal-fired power plants, and industry). Bottom-up technology-based emission inventories (EI) for BC are generally challenged by large uncertainties (100−500%) arising from both activity estimates and emission factors (i.e., kg of BC per ton of burnt fuel).[9,10] Top-down measurements of BC climate effects suggests that EI-based modeling studies underestimate the effects by a factor of 2 to 3.[1,2,11] In addition, comparisons of EI estimates of the fraction biomass versus fossil atmospheric elemental carbon (EC; the mass-based correspondent of BC)[12] with top-down observations of its source-diagnostic isotopic composition suggests a systematic underestimation by EI of the fossil component for the two largest BC emitters, India and China.[13−15] For the Arctic, EI estimates of the fraction biomass for EC reaching north of 60° N ranges from 11%[16] over 48%[9] to 68%[17] (see Table S1), each acknowledging large uncertainties. To improve our understanding of EC sources and source-dependent effects, several studies emphasize the need for observational-based source apportionment studies.[1,18,19]

The application of natural abundance radiocarbon (^{14}C) techniques to carbon-containing aerosols has allowed the resolution of fossil versus biomass sources with high precision.[13,15,20−23] This technique relies on the fact that fossil sources are completely depleted in ^{14}C, whereas (modern) biomass sources have a distinct and well-constrained $^{14}C/^{12}C$ signature, allowing a two end-member computation of the

Received: May 29, 2015
Revised: August 30, 2015
Accepted: September 2, 2015
Published: September 2, 2015

DOI: 10.1021/acs.est.5b02644
Environ. Sci. Technol. 2015, 49, 11959−11966

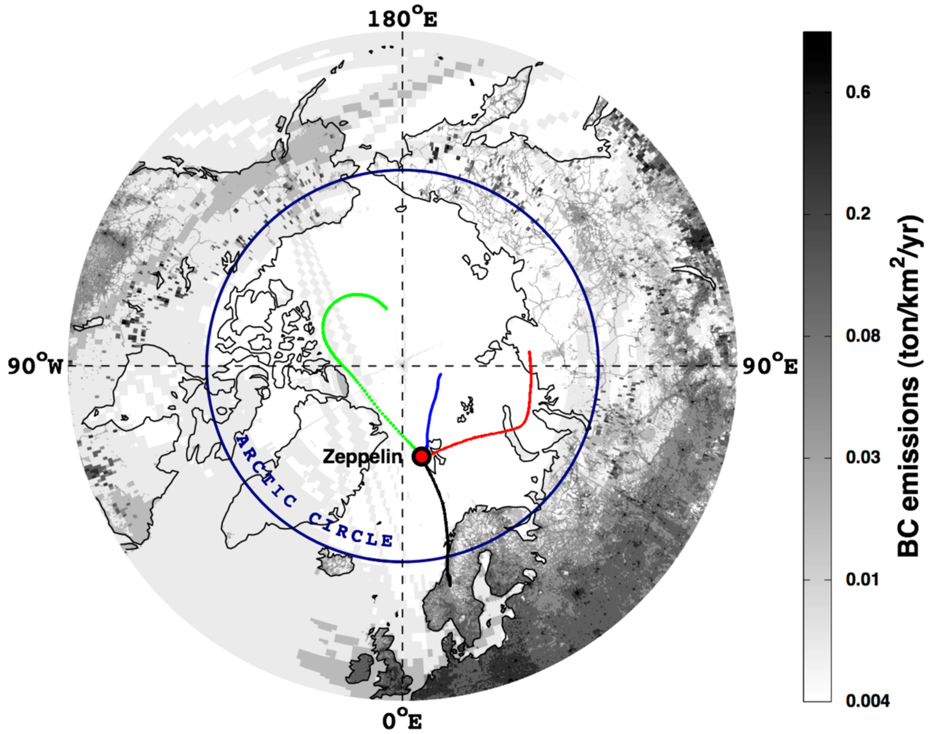

Figure 1. Arctic circumpolar map showing the location of the Zeppelin Observatory on Svalbard (red dot with black circle) and the four mean back-trajectory clusters: Arctic Ocean (blue line), Europe (black line), Northern Siberia (red line), and Northern Greenland and Canada (green line). The BC emission inventory for the year 2008 (Wang et al., 2014)[17] is in gray scale (scale bar).

fraction biomass burning (f_{bb}; with fraction fossil $f_{fossil} = 1 - f_{bb}$). There are three distinct advantages of radiocarbon-based source apportionment, the first being the aforementioned well-defined end-members, which lead to a clear differentiation of fossil and modern sources. Second, it is possible to characterize the radiocarbon signature of specific fractions, e.g., EC, organic carbon (OC), and water-soluble organic carbon (WSOC).[20,23−26] Finally, whereas certain subfractions of carbonaceous aerosols tend to react during transport, recalcitrant EC is expected to be more inert and thereby conserve the source-specific isotope signature.[24] Furthermore, the $^{14}C/^{12}C$ ratio is reported at −25 per mille relative to a $^{13}C/^{12}C$ standard and is thus not affected by isotope-fractionating processes, such as deposition or reactions during atmospheric transport.[20] The two isotopic signatures of $^{14}C/^{12}C$ ($\Delta^{14}C$) and $^{13}C/^{12}C$ ($\delta^{13}C$) can subsequently be combined to a 2D isotope signature with additional source-diagnostic information. For instance, $\delta^{13}C$-EC adds a specific distinction between gaseous fossil (e.g., gas flaring) and liquid fossil (e.g., gasoline and diesel) sources, allowing source differentiation of these contributions.[20]

The current study presents the first radiocarbon-based source apportionment of EC in the Arctic. High-volume PM_{10} filter samples (particulate matter with an aerodynamic equivalent diameter smaller than 10 μm) were collected during 2008 and 2009 at the Zeppelin Observatory on Svalbard (Norway) to elucidate the relative source contributions of EC during high-pollution events in the high European Arctic.

■ MATERIALS AND METHODS

Field Sampling. Quartz fiber filter samples were collected from March 2008 to March 2009 at the Zeppelin Observatory (Figure 1) (11.9° E, 78.9° N, 478 meters above sea level) near Ny-Ålesund, Svalbard (Norway), as part of the POLARCAT (Polar Study using Aircraft, Remote Sensing, Surface Measurements and Models, Climate, Chemistry, Aerosols, and Transport) project.[27,28] The present $^{13}C/^{14}C$-based EC source apportionment study focused on 16 samples, collected during the period of January 6 to March 4 of 2009 (Figure S1), that generally had higher EC loadings than the rest of the sampling period.

EC and OC Measurements. The initial selection of the 16 high-loading filter samples were based on thermal−optical analysis (EUSAAR_2) reported by Yttri and co-workers for a wider set of samples studied in this period[28] (see Table S2). For the detailed isotope-based part of this study, the elemental carbon and organic carbon aerosol concentrations of the 16 samples were measured with a thermal−optical transmission (TOT) analyzer (Sunset Laboratory, Tigard, OR; instrument #227) using the NIOSH 5040 protocol.[29] The filter samples were acidified prior to analysis to remove potential interference from carbonates (by fumigation in open glass Petri dishes held in a desiccator over 12 M hydrochloric acid for 24 h and subsequently dried at 60 °C for 1 h).[13,14,26] None of the two blanks collected during the herein-studied period showed detectable values of EC,[28] which is in agreement with previous observations.[13,20]

Particle Soot Absorption Photometer Black Carbon Measurements and Equivalent Black Carbon Estimates. Measurements of optical black carbon (BC) were obtained using a custom-built particle soot absorption photometer (PSAP), measuring the absorption coefficient (PSAP-BC) at a wavelength of 525 nm (Figure 2). Data were corrected for filter-loading and scattering aerosols following Bond et al. (1999).[30] The corrections utilized, as a first choice, nephelometer (TSI 3563) data when available, or as a second

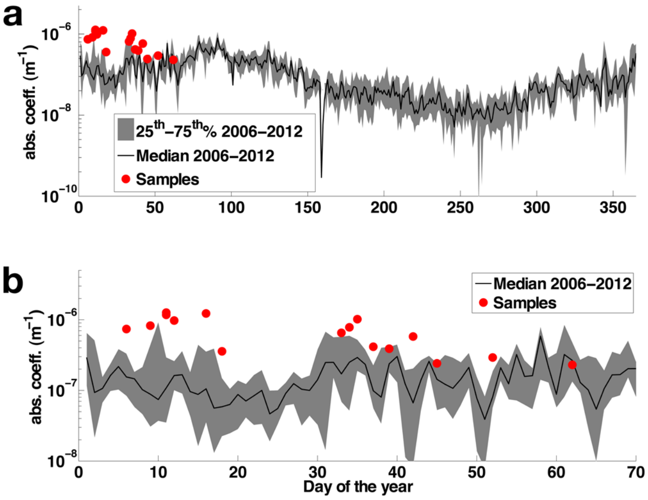

Figure 2. (a) Multiyear annual-cycle PSAP absorption coefficient data (a common metric for BC) for the Zeppelin Observatory based on data from 2006 to 2012, with the 25th and 75th percentile (gray shaded area) and median for 2006–2012 (black line) shown. The figure shows that most of the 16 high-pollution event samples selected for $^{13}C/^{14}C$-EC analysis (red dots) represent PSAP-BC levels above the long-term median. (b) Close up of the Jan–Mar study period.

choice, a scattering coefficient (525 nm) calculated using the Mie theory on a measured aerosol number size distribution between 5 and 800 nm.[31] The PSAP-BC signals were converted to an equivalent black carbon (EBC) metric to allow for a comparison with literature-reported levels using a mass absorption cross-section (MAC) of 10 m^2/g.[7,12,32,33] The scattering Ångström exponent (SAE) and single-scattering albedo (SSA) were derived from PSAP and nephelometer (for the 550–700 nm wavelength pair) observations.

Carbon Isotope Analysis. The selected 16 aerosol high-loading filter samples were combined into 14 samples or composites for determination of their isotopic fingerprint (Table 1). The EC fraction destined for offline isotopic analyses was isolated and cryogenically trapped after conversion to CO_2 using a modified Sunset Laboratory instrument, as previously described.[13] To remove water and halogen-containing gases, which may interfere with the ^{14}C–CO_2 analysis protocol, these coproduced gases were scrubbed online through magnesium perchlorate and silver wool (heated to 550 °C), prior to the cryotrapping in a glass vial suspended in liquid N_2. The collected CO_2 was subsequently reduced to graphite, and the carbon isotopic compositions ($^{14}C/^{12}C$ and $^{13}C/^{12}C$) were measured at the US-NSF National Ocean Science Accelerator Mass Spectrometry (NOSAMS) facility (Woods Hole, MA).[34,35] The $^{14}C/^{12}C$ and $^{13}C/^{12}C$ data were reported on the $\Delta^{14}C$ and $\delta^{13}C$ scales, respectively.[36]

Through the commonly known effect of charring during the anoxic phase of thermal–optical analysis, there is a possibility that parts of the pyrolyzed OC fraction end up as pyrogenic carbon (PC) in the EC fraction. This would lead to an overestimation of the fraction of biomass burning, given that OC is typically of mainly contemporary origin. The potential total available amount of PC can be evaluated by comparing the light attenuation of PC and EC during the TOT analysis (see Table S3 and the Supporting Information text). This shows that, after necessary correction for the relatively higher MAC of PC compared to that of EC, PC and EC are present in roughly equal amounts.[37]

To assess the potential effects of PC transfer into the EC phase, we conducted an isotopic mass balance based sensitivity analysis (see Table S4 and text in the Supporting Information).[13,20] From this estimate, we conclude that even if the PC contribution to EC was as high as 25%, this would lead to a maximum shift in relative biomass burning contribution of 7%.

Hybrid Single Particle Lagrangian Integrated Trajectory Back Trajectories. Back trajectories (BT) were calculated using NOAA's hybrid single particle Lagrangian integrated trajectory (HYSLPLIT) model, software version 4.[38–40] BT measurements of 5 days at two starting heights (474 and 1000 meters above ground level) were generated for every

Table 1. Concentrations and Isotope Measurements for 2009 Wintertime High-EC Loading Events at the Zeppelin Observatory, Svalbard[a]

sampling start date DD.MM.YY	sampling time [h]	$\delta^{13}C$ [‰]	$\Delta^{14}C$ [‰]	EC f_{bb} [%]	EC [ng C m^{-3}]	OC [ng C m^{-3}]	OC/EC	levoglucosan [ng m^{-3}]
06.01.09	22	−25.2 ± 0.1	159 ± 7	95 ± 2	153 ± 74	651 ± 99	4.2	1.7 ± 0.1
09.01.09	27	n/a	−507 ± 5	40 ± 1	329 ± 72	797 ± 95	2.4	6.3 ± 0.3
10.01.09	24	n/a	−367 ± 3	52 ± 1	362 ± 81	895 ± 108	2.5	5.1 ± 0.3
11.01.09	20	−27.0 ± 0.1	−27 ± 6	79 ± 1	283 ± 89	794 ± 114	2.8	9.8 ± 0.5
12.01.09	23	−25.8 ± 0.1	−521 ± 2	39 ± 1	309 ± 79	890 ± 108	2.9	3.4 ± 0.2
16.01.09	28	−27.9 ± 0.1	−468 ± 3	43 ± 1	496 ± 78	992 ± 102	2.0	8.9 ± 0.4
17.01.09	25	−27.5 ± 0.1	−426 ± 4	47 ± 1	179 ± 70	784 ± 100	4.4	10.4 ± 0.5
02.02.09	24	−23.9 ± 0.1	−476 ± 2	43 ± 1	174 ± 71	864 ± 105	5.0	7.7 ± 0.4
03.02.09	24	−24.7 ± 0.1	−67 ± 3	76 ± 1	236 ± 74	902 ± 107	3.8	7 ± 0.4
04.02.09	24	−20.1 ± 0.1	−64 ± 4	76 ± 1	196 ± 72	989 ± 111	5.0	7.6 ± 0.4
06.02.09	28				composite			
07.02.09	25	−24.4 ± 0.1	201 ± 3	98 ± 1	90 ± 61	578 ± 86	6.5	4.1 ± 0.2
11.02.09	25				composite 2			
13.02.09	30	−26.0 ± 0.1	−347 ± 2	53 ± 1	75 ± 58	387 ± 74	5.2	6.2 ± 0.3
20.02.09	66	−26.5 ± 0.1	−471 ± 6	43 ± 1	51 ± 25	253 ± 36	5.0	1.6 ± 0.1
03.03.09	23	−23.2 ± 0.1	−346 ± 4	53 ± 1	87 ± 68	540 ± 90	6.2	1.9 ± 0.1

[a] The fraction biomass burning (f_{bb}) was calculated from the ambient $\Delta^{14}C$ data using a biomass burning end-member of +225 ± 25‰. Levoglucosan data was adapted from Yttri et al. (2014).[28]

6 h during January, February, and March of 2009. These BTs were sorted into four bins using cluster analysis: (I) Europe, (II) North Siberia, (III) North Greenland and North Canada, and (IV) the Arctic Ocean (Figure 1 and Figures S2−S6). The geographical source region for each sample-collection period was examined by overlaying the results from the BT cluster analysis with the filter sampling periods (Figure 3). In addition, 16 BTs (8 days at 474 and 1000 meters above ground level) were computed for every single sample (see Figures S7−S20).

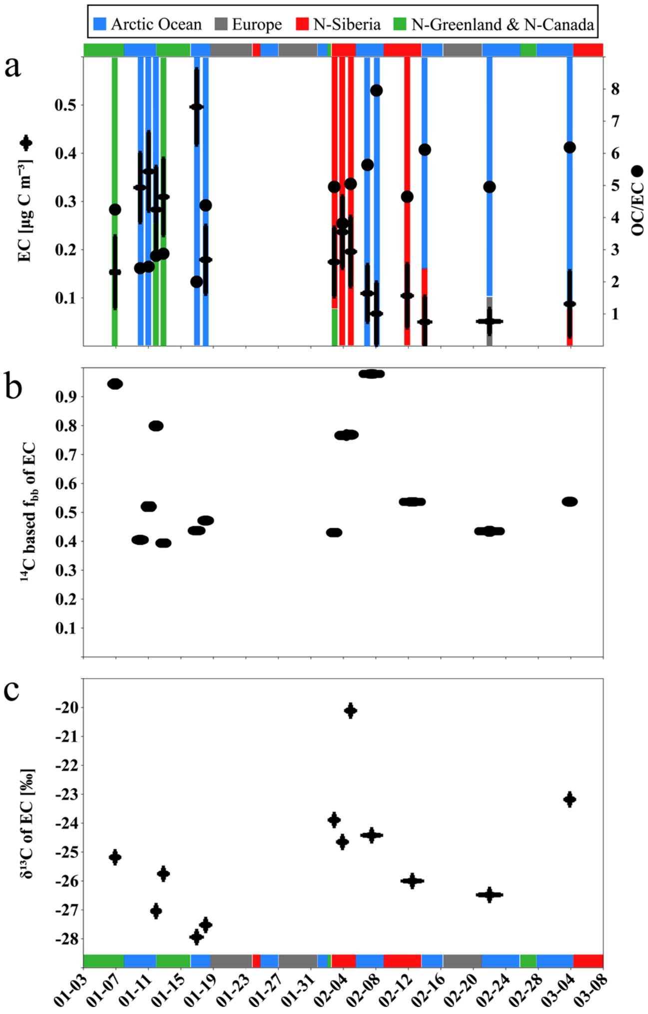

Figure 3. Temporal variation in EC concentration and isotopic composition during high-loading episodes at the Zeppelin Observatory during the winter of 2009. (A) EC concentrations (crosses) of all 16 samples, where the error bars indicate analytical precision and horizontal bars indicate sampling duration. The OC/EC ratios are indicated with dots. The colored line corresponding to each data point shows the attribution to source cluster in fractions. (B) ^{14}C-based fraction biomass burning (f_{bb}) of EC for 14 composites with error bars (1 = 100% biomass). (C) Stable isotope (δ^{13}C) data from 14 composites.

Isotopic Mass Balance Equation. The fractional contributions from biomass (f_{bb}) versus fossil ($f_{fossil} = 1 - f_{bb}$) sources to these Arctic EC samples were resolved from Δ^{14}C by an isotopic mass balance equation:[14]

$$\Delta^{14}C_{sample} = \Delta^{14}C_{biomass} \cdot f_{bb} + \Delta^{14}C_{fossil} \cdot (1 - f_{bb}) \qquad (1)$$

where $\Delta^{14}C_{sample}$ represents the radiocarbon signature in the ambient samples. The $\Delta^{14}C_{fossil}$ is −1000‰ by definition because fossil carbon is completely depleted in radiocarbon. The end-members for $\Delta^{14}C_{biomass}$ are dependent on the type and age of the studied biomass. The most common wintertime sources for biomass BC in the Arctic region is wood burning, for which recent studies suggest using an end-member with a Δ^{14}C value ranging from +189 to +264‰ for typical Northern tree species such as pine and birch.[13,14,41−45] To account for this variability in the biomass Δ^{14}C end-member, we ran Monte Carlo simulations to estimate the resulting uncertainties in the calculated fraction biomass.[46] By representing the biomass Δ^{14}C end-member as a normal distribution with a mean of +225‰ and a standard deviation of 25‰, we find that this variability results in an uncertainty in the calculated fraction biomass by a maximum of 1% for the different samples.

■ RESULTS AND DISCUSSION

Meteorological Setting and Air Mass Characterization. The meteorology of the Zeppelin Observatory is influenced by the Arctic Oscillation (AO).[47,48] A positive AO facilitates cyclonic conditions and hence is expected to enhance wind transport from North America and Europe into the Arctic.[48,49] Overall, the year 2009 experienced negative values in the AO. However, the samples addressed in the current study were collected in a period when the AO was in a positive phase or near zero. During the studied months of 2009, the air masses arriving at the Zeppelin Observatory were binned into four BT clusters: the Arctic Ocean (44% of the time), Europe (27%), North Siberia (15%), and Northern Greenland and Canada (14%) (Figure 1). The air masses for the herein discussed samples, however, originated, in the nearest preceding time, mainly from the Arctic Ocean cluster (53%) (Figure 3), circulating for more than 5 days inside the Arctic vortex. For these cases, a more in-depth discussion on geographical origin is only possible by looking at single BTs of more than 5 days (see single BTs in Figures S7−S20).

Levels of Carbonaceous Aerosols Observed at the Zeppelin Observatory. Long-term records of EBC concentrations at the Zeppelin Observatory and other Arctic stations reveal a strong seasonal variability, with enhanced levels during the winter−spring "haze" periods.[50,51] In addition to this seasonality, there is also a strong variability of higher temporal frequency (hours to days), with occasional "plumes" influencing the observatory.[7,52,53] The levels of the selected high-loading samples of the present study were above a 6 year average (2006−2012) of light-absorption-based PSAP-BC levels (Figure 2). This is also reflected in the observed high EC concentrations for the selected samples. The temporal trends in EC (mass-based analyses) and the PSAP-BC observations (direct optical metric) are in good agreement (R^2 = 0.76). The mean EBC concentration (70 ± 35 ng m^{-3}) for the 16 samples was higher than the annual mean (39 ng m^{-3}) reported for the Zeppelin Observatory for the period of 1998−2007,[50] yet it is comparable to the mean concentration reported for February (80 ng m^{-3}) during the same time period. February is typically the month with the highest monthly mean BC levels at the Zeppelin Observatory (Figure 2). Pollution events observed during the Arctic haze period have frequently been shown to reach higher concentrations (<300 ng m^{-3}).[50] The highest observed short-term (hourly mean) EBC concentration reported for the European Arctic winter in recent years is 850 ng m^{-3},[52] whereas even higher values have been reported for other parts of the Arctic.[52] The observed EC concentrations for the 16 high-pollution-episode samples (for sampling time, see Table 1) have a mean concentration of 230 ± 120 ng C m^{-3}, ranging from 50 to 500 ng C m^{-3} (Figure 3). Organic carbon (OC) concentrations have a mean value of 710 ± 230 ng C m^{-3}, with a range from 250 to 990 ng C m^{-3} (OC values are not blank-corrected).

δ^{13}C and Δ^{14}C Source Fingerprinting of High Arctic EC. The carbon isotope signatures of EC provide observational-based insights into the sources of BC. In particular, the Δ^{14}C signature facilitates a direct quantification of biomass versus fossil sources (eq 1). The Δ^{14}C values of all 14 composites (composed of 16 samples) range between −521 and +201‰ (Table 1), corresponding to a fraction biomass burning ranging from 39% to 98% (57 ± 21%; Figure 3). The two major groups of samples or composites formed are, (I) slightly dominated by fossil fuel combustion, with f_{bb} values ranging from 39% to 53% (46 ± 5%), and (II) strongly dominated by biomass burning, ranging from 76% to 98% (85 ± 9%). However, there are no clear temporal or geographical trends in the back trajectories of these two groups. Both groups are represented in all four BT source clusters. This highlights the complexity of BC in the Arctic atmosphere, where the generally low BC levels may be strongly influenced by point sources or occasional combustion practices.

High levels of EBC dominated by wild and agricultural fires have previously been reported for the Zeppelin Observatory.[52] However, this is the first time that EC dominated by biomass burning has been reported in winter, during which emissions from residential heating are likely the major biomass burning source. A pair of the samples or composites are enriched in Δ^{14}C to such an extent that their EC content appear to be nearly exclusively originating from biomass burning, i.e., a f_{bb} value of 95% on January 6 and a f_{bb} value of 98% on February 7 (Table 1). The chemical composition of these samples or composites were very different from the others (for a complete list of auxiliary chemical tracers, optical measurements, and their values, see Tables S5 and S6). January 6 has the highest biomass-indicative potassium/EC ratio of all samples (see Figure S28) and low fossil-fuel-associated metal concentrations (cadmium, lead, manganese, and vanadium). In addition, this sample is characterized by low levoglucosan/EC (see Figure S21) and SAE/SSA (see Figure S24) ratios. In contrast, the composite collected on February 6 (f_{bb} = 98%) exhibited very high ratios of typical anthropogenic trace metals (cadmium, manganese, lead, and vanadium) to EC compared to those of all other samples (see Figures S21−S32), while ratios of typical biomass indicators such as potassium and levoglucosan were low.[54−56] Thus, the January 6 sample has the typical source characteristics of a nonwood biomass burning source. A low SAE/SSA ratio indicates large particles, typically representing a local emissions source, potentially cigarette smoke. The very high f_{bb} (February 6) sample is characterized by typical nonbiomass chemical features. We note that observations of ^{14}C enrichment due to minute emissions of radiogenic emissions from, e.g., nuclear reactors or the burning of ^{14}C-labeled medical research waste have been observed in the North European atmosphere.[57−59] Hence, it cannot be excluded that the f_{bb} value of 98% for this sample is somehow affected by an admixture of a radiogenic source with artificially high ^{14}C/^{12}C ratios and should be excluded from a final (conservative) estimate of f_{bb}. In either case, the inclusion or exclusion of these two high-f_{bb} samples or composites does not significantly change the overall ^{14}C-based source apportionment results for the wintertime Zeppelin Observatory EC high-pollution events; both fossil fuel and biomass combustion are contributing substantially. Fraction biomass combustion is 57 ± 21% when the full 14 observations are taken into account, while if these two ^{14}C-rich plumes are excluded, the fraction biomass burning becomes 52 ± 15%.

In addition to Δ^{14}C, complementary information regarding the sources of EC is available from the characterization of the stable carbon isotopic signature (δ^{13}C). For organic aerosols the δ^{13}C signature has recently been found to be highly influenced by effects of atmospheric processing.[21,25,26] In contrast, one of the defining properties of EC (BC) is the recalcitrance to chemical or physical transformations.[60,61] The δ^{13}C-EC signal is thus changing much less during long-range transport. As a consequence, the δ^{13}C signature of EC is an indicator of emissions sources.[20] However, in contrast to Δ^{14}C, the end-member values for δ^{13}C are not as well-constrained because there are more than two distinct source classes that have partially overlapping source profiles.

For the present study, the average value for all available δ^{13}C measurements is −25.2 ± 2.1‰, with a range from −20.1 to −27.9‰ (Table 1). Considerable temporal variability in the δ^{13}C-EC signature is observed (Figure 3c), which is in agreement with what has been reported by others in, e.g., Asia[13,20,21] and North America.[24] The mean δ^{13}C-EC signature for January (−26.7 ± 1.1‰) appears depleted relative to that of February (−24.1 ± 2.0‰), pointing to a shift in combustion sources, which in turn reflects a shift in the source regions. The January signatures are consistent with a biomass burning signature (i.e., C3 plant; ^{13}C ≈ −26.7 ± 1.8‰)[20] or potential influences from gas-flaring activities (δ^{13}C values from −36 to −40‰),[62] whereas the more enriched values from February indicate the influence of coal combustion (δ^{13}C ≈ −23.4 ± 1.3‰).[20] Liquid fossil sources (e.g., petroleum, gasoline, and oil) are characterized by intermediate values (δ^{13}C ≈ −25.5 ± 1.3‰).[20] The January samples or composites are mainly influenced by the two clusters from the Arctic Ocean, and Northern Greenland and Canada, while February samples are dominated by the Arctic Ocean and the North Siberian clusters (Figure 3). The February 4 δ^{13}C signature (−20.1‰) is the most enriched for all samples or composites. Even though it has similar source regions as other samples (e.g., February 2, 3, and 6), it does not share their isotopic characteristics. Although such values are not uncommon,[20,24] it is not clear what source this value would represent in the Arctic context.

δ^{13}C/Δ^{14}C-Based Statistical Source Apportionment of High Arctic EC. Combining Δ^{14}C and δ^{13}C provides a powerful tool for the investigation of sources. With the exception of the highly ^{13}C-enriched February 4 sample, all data points fall reasonably well within the "source triangle" of the expected three major sources: C3 plants, coal, and liquid fossil fuels (Figure 4). There is considerable variability in both isotope dimensions, yet no samples are observed with Δ^{14}C below −600‰ (corresponding to f_{bb} = 33%), indicating significant biomass burning contributions throughout, with an average f_{bb} value of 52 ± 15% (discounting the samples from January 6 and February 6).

A recent study, coupling bottom-up BC emission inventory with a transport model, suggests that gas-flaring activities, from mainly the Kara Sea region in northern Russia, may account for up to 42% of the year-round BC in the Arctic.[28] Isotopes give an opportunity to test the feasibility of a large contribution

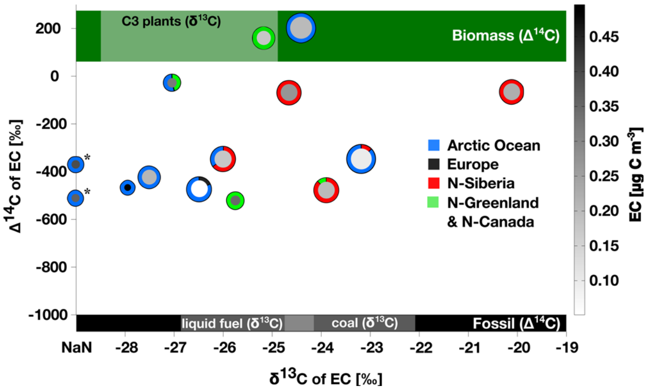

Figure 4. Isotope-based 2D source characterization of EC aerosols at Zeppelin Observatory during high-pollution wintertime events in 2009. The δ^{13}C source-signature ranges (mean ± standard deviation) for C3 plants, liquid fossils, and coal are outlined with light shading within the Δ^{14}C-based end-member ranges for biomass combustion (green, top) and fossil fuel combustion (gray, bottom).[17] Pure fossil EC would fall inside the black and gray area, while pure biomass EC would fall on the upper edge of the green and light green area. The circle centers in gray scale indicate EC concentrations (scale to the right), and their diameter represents OC/EC ratios from 2 to 6.5. The outer colors of the rings indicate source regions as determined by back-trajectory cluster analysis. Samples for which no δ^{13}C data are available are plotted on the *y*-axis and marked with an asterisk.

from gas flaring. The 2D carbon isotope signature of a sample heavily influenced by gas flaring would be characterized by depletion in both ^{14}C and ^{13}C (Δ^{14}C ≈ −1000‰ and δ^{13}C < −30‰). The sample with the most-depleted δ^{13}C signature (−27.9‰), from January 16, also has the highest EC loading (496 ng C m^{-3}) and the lowest OC/EC ratio (2.0) but a ^{14}C-based fraction biomass of 43%, thus constraining a contribution from all fossil fuel sources, including gas flaring, to 57% for this sample. A BT analysis suggests air-mass transport from over the Kara Sea region during this sampling period. This sample is therefore consistent with a substantial gas-flaring component mixed with a substantial wood-burning contribution, which is in line with the comparably high levoglucosan/EC ratio (0.02; Table 1).[28] However, for the other 13 investigated samples, the dual-carbon isotope characterization of EC suggests that there are no major contributions from gas flaring.

The present dual-carbon isotope-based source characterization of EC at the Zeppelin Observatory targeted high-loading periods that stand for a large fraction of the total BC loadings of the high Arctic. The substantial variability between individual observations in deduced sources is likely a consequence of the overall low-loading regime, where single plumes result in larger effects, as compared to receptor sites with much higher overall loadings, where concentrations and source signals are composed of a greater mixture of multiple sources and, thus, overall much less variable.[13,20,21] While these events only covered 32% of the total sampling time (January through March of 2009 at Zeppelin Observatory), they contributed 74% of the total EC loading for the actual period. Because it is believed that a substantial, if not the largest, climate effect of BC in the Arctic is through the lowering of the surface albedo by deposition on snow and ice,[6,63,64] which reflects the total BC loading, it is noteworthy that the contribution from high-loading events is expected to be large. This variability complicates modeling efforts based on bottom-up emission inventories beyond their inherent challenges (e.g., of variable emission factors) because the comparably large impact from events or point sources is difficult to capture within the framework of existing geographically and temporally coarse-grained resolved bottom-up emission inventories. Nevertheless, here the high-loading events represent the majority of the late-winter EC loading. The quantitative constraint is that slightly more than half of the EC stems from biomass combustion. Although year-round studies at pan-Arctic locations are desirable as a next step, the current results place improved constraints on the sources of BC to the high European Arctic, which benefits both the studies of source-dependent effects of BC on the regional Arctic climate and provide an underpinning for the analysis of BC mitigation efforts.

■ ASSOCIATED CONTENT

Ⓢ Supporting Information

The Supporting Information is available free of charge on the ACS Publications website at DOI: 10.1021/acs.est.5b02644.

> Tables S1−S6 list literature values for emission inventories, concentration data (EUSAAR_2) for all samples collected during the campaign, an estimate for the influence of pyrolysis on EC, a sensitivity study for pyrogenic carbon, a list of all auxiliary chemical tracers obtained via the EBAS database, and their concentrations. Figures S1−S32 show a selection of samples, various back trajectories and various components (chemical tracers) measured at the Zeppelin Observatory. (PDF)

■ AUTHOR INFORMATION

Corresponding Author

*Phone: +46 8 674 7317; fax: +46 8 674 7638; e-mail: orjan.gustafsson@aces.su.se.

Author Contributions

The manuscript was written through contributions of all authors. All authors have given approval to the final version of the manuscript.

Notes

The authors declare no competing financial interest.

■ ACKNOWLEDGMENTS

A.A., Ö.G., and P.W. acknowledge financial support from the Swedish Energy Agency (contract number 35450-2) and the European Union under the 7th Framework Programme (project acronym: CSI:ENVIRONMENT; contract number PITN-GA-2010-264329). The work of K.E.Y. was further supported by the EU 7th Framework Program ECLIPSE project (grant agreement number 282688). The authors gratefully acknowledge NOAA ARL for use of HYSPLIT. NILU's atmospheric monitoring program at the Zeppelin Observatory is financed by the Norwegian Environment Agency. The data are submitted to the EMEP and AMAP programs and is available from http://ebas.nilu.no/. Thanks are extended to the staff at the Norwegian Polar Institute and NILU. This study also benefited from the research environment provided by the Bolin Centre for Climate Research at the Stockholm University School of Natural Sciences.

■ REFERENCES

(1) Bond, T. C.; Doherty, S. J.; Fahey, D. W.; Forster, P. M.; Berntsen, T.; Deangelo, B. J.; Flanner, M. G.; Ghan, S.; Kärcher, B.;

Koch, D.; et al. Bounding the role of black carbon in the climate system: A scientific assessment. *J. Geophys. Res. Atmos.* **2013**, *118* (11), 5380−5552.

(2) Andreae, M. O.; Ramanathan, V. Climate's Dark Forcings. *Science* **2013**, *340* (6130), 280−281.

(3) Boucher, O.; Randall, D.; Artaxo, P.; Bretherton, C.; Feingold, G.; Forster, P.; Kerminen, V.-M.; Kondo, Y.; Liao, H.; Lohmann, U.7. Clouds and Aerosols. In *Climate Change 2013: The Physical Science Basis. Contribution of Working Group I to the Fifth Assessment Report of the Intergovernmental Panel on Climate Change*; Cambridge University Press: New York, 2013; pp 571−657.

(4) Garrett, T. J.; Brattström, S.; Sharma, S.; Worthy, D. E. J.; Novelli, P. The role of scavenging in the seasonal transport of black carbon and sulfate to the Arctic. *Geophys. Res. Lett.* **2011**, *38* (16), GB3016.

(5) Hirdman, D.; Burkhart, J. F.; Sodemann, H.; Eckhardt, S.; Jefferson, A.; Quinn, P. K.; Sharma, S.; Ström, J.; Stohl, A. Long-term trends of black carbon and sulphate aerosol in the Arctic: Changes in atmospheric transport and source region emissions. *Atmos. Chem. Phys.* **2010**, *10* (19), 9351−9368.

(6) Quinn, P. K.; Bates, T. S.; Baum, E.; Doubleday, N.; Fiore, A. M.; Flanner, M.; Fridlind, A.; Garrett, T. J.; Koch, D.; Menon, S.; et al. Short-lived pollutants in the Arctic: their climate impact and possible mitigation strategies. *Atmos. Chem. Phys.* **2008**, *8* (7), 1723−1735.

(7) Stohl, A.; Klimont, Z.; Eckhardt, S.; Kupiainen, K.; Shevchenko, V. P.; Kopeikin, V. M.; Novigatsky, A. N. Black carbon in the Arctic: the underestimated role of gas flaring and residential combustion emissions. *Atmos. Chem. Phys.* **2013**, *13* (17), 8833−8855.

(8) Eckhardt, S.; Quennehen, B.; Olivié, D. J. L.; Berntsen, T. K.; Cherian, R.; Christensen, J. H.; Collins, W.; Crepinsek, S.; Daskalakis, N.; Flanner, M.; et al. Current model capabilities for simulating black carbon and sulfate concentrations in the Arctic atmosphere: a multi-model evaluation using a comprehensive measurement data set. *Atmos. Chem. Phys. Discuss.* **2015**, *15* (7), 10425−10477.

(9) Bond, T. C.; Streets, D. G.; Yarber, K. F.; Nelson, S. M.; Woo, J. H.; Klimont, Z. A technology-based global inventory of black and organic carbon emissions from combustion. *J. Geophys. Res.* **2004**, *109*, D14203.

(10) Zhao, Y.; Nielsen, C. P.; Lei, Y.; McElroy, M. B.; Hao, J. Quantifying the uncertainties of a bottom-up emission inventory of anthropogenic atmospheric pollutants in China. *Atmos. Chem. Phys.* **2011**, *11* (5), 2295−2308.

(11) Cohen, J. B.; Wang, C. Estimating global black carbon emissions using a top-down Kalman Filter approach. *J. Geophys. Res. Atmos.* **2014**, *119* (1), 307−323.

(12) Petzold, A.; Ogren, J. A.; Fiebig, M.; Laj, P.; Li, S. M.; Baltensperger, U.; Holzer-Popp, T.; Kinne, S.; Pappalardo, G.; Sugimoto, N.; et al. Recommendations for reporting black carbon measurements. *Atmos. Chem. Phys.* **2013**, *13* (16), 8365−8379.

(13) Chen, B.; Andersson, A.; Lee, M.; Kirillova, E. N.; Xiao, Q.; Kruså, M.; Shi, M.; Hu, K.; Lu, Z.; Streets, D. G.; et al. Source forensics of black carbon aerosols from China. *Environ. Sci. Technol.* **2013**, *47* (16), 9102−9108.

(14) Gustafsson, O.; Kruså, M.; Zencak, Z.; Sheesley, R. J.; Granat, L.; Engström, E.; Praveen, P. S.; Rao, P. S. P.; Leck, C.; Rodhe, H. Brown clouds over South Asia: biomass or fossil fuel combustion? *Science* **2009**, *323* (5913), 495−498.

(15) Zhang, Y.-L.; Huang, R.-J.; El Haddad, I.; Ho, K.-F.; Cao, J.-J.; Han, Y.; Zotter, P.; Bozzetti, C.; Daellenbach, K. R.; Canonaco, F.; et al. Fossil vs. non-fossil sources of fine carbonaceous aerosols in four Chinese cities during the extreme winter haze episode of 2013. *Atmos. Chem. Phys.* **2015**, *15* (3), 1299−1312.

(16) Amann, M.; Bertok, I.; Borken-Kleefeld, J.; Cofala, J.; Heyes, C.; Höglund-Isaksson, L.; Klimont, Z.; Nguyen, B.; Posch, M.; Rafaj, P.; et al. Cost-effective control of air quality and greenhouse gases in Europe: Modeling and policy applications. *Environ. Model. Softw.* **2011**, *26* (12), 1489−1501.

(17) Wang, R.; Tao, S.; Balkanski, Y.; Ciais, P.; Boucher, O.; Liu, J.; Piao, S.; Shen, H.; Vuolo, M. R.; Valari, M.; et al. Exposure to ambient black carbon derived from a unique inventory and high-resolution model. *Proc. Natl. Acad. Sci. U. S. A.* **2014**, *111* (7), 2459−2463.

(18) Lawrence, M. G.; Lelieveld, J. Atmospheric pollutant outflow from southern Asia: A review. *Atmos. Chem. Phys.* **2010**, *10* (22), 11017−11096.

(19) UNEP; WMO. *Integrated Assessment of Black Carbon and Tropospheric Ozone*; UNON/Publishing Services Section: Nairobi, Kenya, 2011.

(20) Andersson, A.; Deng, J.; Du, K.; Yan, C.; Zheng, M.; Sköld, M.; Gustafsson, O. Regionally-varying combustion sources of the January 2013 severe haze events over eastern China. *Environ. Sci. Technol.* **2015**, *49* (4), 2038−2043.

(21) Bosch, C.; Andersson, A.; Kirillova, E. N.; Budhavant, K.; Tiwari, S.; Praveen, P. S.; Russell, L. M.; Beres, N. D.; Ramanathan, V.; Gustafsson, Ö. Source-diagnostic dual-isotope composition and optical properties of water-soluble organic carbon and elemental carbon in the South Asian outflow intercepted over the Indian Ocean. *J. Geophys. Res. Atmos.* **2014**, *119*, 11743−11759.

(22) Clayton, G. D.; Arnold, J. R.; Patty, F. A. Determination of Sources of Particulate Atmospheric Carbon. *Science* **1955**, *122* (3173), 751−753.

(23) Szidat, S.; Jenk, T. M.; Gäggeler, H. W.; Synal, H. A.; Fisseha, R.; Baltensperger, U.; Kalberer, M.; Samburova, V.; Reimann, S.; Kasper-Giebl, A.; et al. Radiocarbon (14C)-deduced biogenic and anthropogenic contributions to organic carbon (OC) of urban aerosols from Zürich, Switzerland. *Atmos. Environ.* **2004**, *38* (24), 4035−4044.

(24) Huang, L.; Brook, J. R.; Zhang, W.; Li, S. M.; Graham, L.; Ernst, D.; Chivulescu, A.; Lu, G. Stable isotope measurements of carbon fractions (OC/EC) in airborne particulate: A new dimension for source characterization and apportionment. *Atmos. Environ.* **2006**, *40* (15), 2690−2705.

(25) Kirillova, E. N.; Andersson, A.; Sheesley, R. J.; Kruså, M.; Praveen, P. S.; Budhavant, K.; Safai, P. D.; Rao, P. S. P.; Gustafsson, Ö. 13C- And 14C-based study of sources and atmospheric processing of water-soluble organic carbon (WSOC) in South Asian aerosols. *J. Geophys. Res. Atmos.* **2013**, *118* (2), 614−626.

(26) Kirillova, E. N.; Andersson, A.; Han, J.; Lee, M.; Gustafsson, Ö. Sources and light absorption of water-soluble organic carbon aerosols in the outflow from northern China. *Atmos. Chem. Phys.* **2014**, *14* (3), 1413−1422.

(27) Law, K. S.; Stohl, A.; Quinn, P. K.; Brock, C.; Burkhart, J.; Paris, J. D.; Ancellet, G.; Singh, H. B.; Roiger, A.; Schlager, H.; et al. Arctic Air Pollution: New Insights From POLARCAT-IPY. *Bull. Am. Meteorol. Soc.* **2014**, *95*, 1873−1895.

(28) Yttri, K. E.; Lund Myhre, C.; Eckhardt, S.; Fiebig, M.; Dye, C.; Hirdman, D.; Ström, J.; Klimont, Z.; Stohl, A. Stohl, a. Quantifying black carbon from biomass burning by means of levoglucosan - A one-year time series at the Arctic observatory Zeppelin. *Atmos. Chem. Phys.* **2014**, *14* (12), 6427−6442.

(29) Birch, M. E.; Cary, R. A. Elemental Carbon-Based Method for Monitoring Occupational Exposures to Particulate Diesel Exhaust. *Aerosol Sci. Technol.* **1996**, *25* (3), 221−241.

(30) Bond, T. C.; Anderson, T. L.; Campbell, D. Calibration and Intercomparison of Filter-Based Measurements of Visible Light Absorption by Aerosols. *Aerosol Sci. Technol.* **1999**, *30* (6), 582−600.

(31) Wiscombe, W. J.; Warren, S. G. A model for the spectral albedo of snow. I: Pure snow. *J. Atmos. Sci.* **1980**, *37*, 2712−2733.

(32) Bond, T. C.; Bergstrom, R. W. Light Absorption by Carbonaceous Particles: An Investigative Review. *Aerosol Sci. Technol.* **2006**, *40* (1), 27−67.

(33) Stohl, A. Characteristics of atmospheric transport into the Arctic troposphere. *J. Geophys. Res.* **2006**, *111*, D11306.

(34) McNichol, A. P.; Gagnon, A. R.; Jones, G. A.; Osborne, E. A. Illumination of a Black Box: Analysis of Gas Composition During Graphite Target Preparation. *Radiocarbon* **1992**, *34* (3), 321−329.

(35) Pearson, A.; Mcnichol, A. P.; Schneider, R. J.; von Reden, K. F.; Zheng, Y. Microscale AMS 14C measurement at NOSAMS. *Radiocarbon* **1998**, *40* (1), 61−75.

(36) Zencak, Z.; Reddy, C. M.; Teuten, E. L.; Xu, L.; McNichol, A. P.; Gustafsson, Ö. Evaluation of gas chromatographic isotope fractionation and process contamination by carbon in compound-specific radiocarbon analysis. *Anal. Chem.* **2007**, *79* (5), 2042−2049.

(37) Chow, J. C.; Watson, J. G. PM 2.5 carbonate concentrations at regionally representative Interagency Monitoring of Protected Visual Environment sites. *J. Geophys. Res.* **2002**, *107* (D21), 8344.

(38) Draxler, R. R.; Hess, G. D. *Description of the HYSPLIT_4 modeling system*; Technical Memorandum ERL ARL-224 for NOAA: Silver Spring, MD, December 1997.

(39) Draxler, R. R.; Hess, G. D. An overview of the HYSPLIT_4 modeling system of trajectories, dispersion, and deposition. *Aust. Meteorol. Mag.* **1998**, *47* (4), 295−308.

(40) Draxler, R. R. *HYSPLIT _ 4 user's guide*; NOAA Technical Memorandum ERL ARL-230; Silver Spring, MD, 1999.

(41) Sheesley, R. J.; Kruså, M.; Krecl, P.; Johansson, C.; Gustafsson, Ö. Source apportionment of elevated wintertime PAHs by compound-specific radiocarbon analysis. *Atmos. Chem. Phys.* **2009**, *9* (10), 3347−3356.

(42) Voorhees, K. J.; Schulz, W. D.; Kunen, S. M.; Hendricks, L. J.; Currie, L. A.; Klouda, G. A. Analysis of insoluble carbonaceous materials from airborne particles collected in pristine regions of colorado. *J. Anal. Appl. Pyrolysis* **1991**, *18* (3−4), 189−205.

(43) Klinedinst, D. B.; Currie, L. A. Direct Quantification of PM 2.5 Fossil and Biomass Carbon within the Northern Front Range Air Quality Study's Domain. *Environ. Sci. Technol.* **1999**, *33* (23), 4146−4154.

(44) Zencak, Z.; Elmquist, M.; Gustafsson, Ö. Quantification and radiocarbon source apportionment of black carbon in atmospheric aerosols using the CTO-375 method. *Atmos. Environ.* **2007**, *41* (36), 7895−7906.

(45) Szidat, S.; Jenk, T. M.; Synal, H. A.; Kalberer, M.; Wacker, L.; Hajdas, I.; Kasper-Giebl, A.; Baltensperger, U. Contributions of fossil fuel, biomass-burning, and biogenic emissions to carbonaceous aerosols in Zurich as traced by 14C. *J. Geophys. Res.* **2006**, *111* (7), 206.

(46) Andersson, A. A systematic examination of a random sampling strategy for source apportionment calculations. *Sci. Total Environ.* **2011**, *412*, 232−238.

(47) Eckhardt, S.; Stohl, A.; Beirle, S.; Spichtinger, N.; James, P.; Forster, C.; Junker, C.; Wagner, T.; Platt, U.; Jennings, S. G. The North Atlantic Oscillation controls air pollution transport to the Arctic. *Atmos. Chem. Phys.* **2003**, *3* (6), 1769−1778.

(48) Macdonald, R. W.; Harner, T.; Fyfe, J. Recent climate change in the Arctic and its impact on contaminant pathways and interpretation of temporal trend data. *Sci. Total Environ.* **2005**, *342* (1−3), 5−86.

(49) L'Heureux, M.; Butler, A.; Jha, B.; Kumar, A.; Wang, W. Unusual extremes in the negative phase of the Arctic Oscillation during 2009. *Geophys. Res. Lett.* **2010**, *37* (10), 704.

(50) Eleftheriadis, K.; Vratolis, S.; Nyeki, S. Aerosol black carbon in the European Arctic: Measurements at Zeppelin station, Ny-Ålesund, Svalbard from 1998−2007. *Geophys. Res. Lett.* **2009**, *36* (2), 809.

(51) Sharma, S.; Andrews, E.; Barrie, L. A.; Ogren, J. A.; Lavoué, D. Variations and sources of the equivalent black carbon in the high Arctic revealed by long-term observations at Alert and Barrow: 1989−2003. *J. Geophys. Res.* **2006**, *111* (14), 208.

(52) Stohl, A.; Berg, T.; Burkhart, J. F.; Fjæraa, A. M.; Forster, C.; Herber, A.; Hov, Ø.; Lunder, C.; McMillan, W. W.; Oltmans, S.; et al. Arctic smoke − record high air pollution levels in the European Arctic due to agricultural fires in Eastern Europe in spring 2006. *Atmos. Chem. Phys.* **2007**, *7* (2), 511−534.

(53) Tunved, P.; Ström, J.; Krejci, R. Arctic aerosol life cycle: linking aerosol size distributions observed between 2000 and 2010 with air mass transport and precipitation at Zeppelin station, Ny-Ålesund, Svalbard. *Atmos. Chem. Phys.* **2013**, *13* (7), 3643−3660.

(54) Andreae, M. O. Soot carbon and excess fine potassium: long-range transport of combustion-derived aerosols. *Science* **1983**, *220* (4602), 1148−1151.

(55) EMEP. *EMEP particulate matter assessment report*; Norwegian Institute for Air Research: Kjeller, Norway, 2007.

(56) Hildemann, L. M.; Markowski, G. R.; Cass, G. R. Chemical composition of emissions from urban sources of fine organic aerosol. *Environ. Sci. Technol.* **1991**, *25* (4), 744−759.

(57) Svetlik, I.; Fejgl, M.; Tomaskova, L.; Turek, K.; Michalek, V. 14C studies in the vicinity of the Czech NPPs. *J. Radioanal. Nucl. Chem.* **2012**, *292*, 689−695.

(58) Vogel, F. R.; Levin, I.; Worthy, D. E. J. Implications for Deriving Regional Fossil Fuel CO2 Estimates from Atmospheric Observations in a Hot Spot of Nuclear Power Plant 14CO2 Emissions. *Radiocarbon* **2013**, *55* (3−4), 1556−1572.

(59) Yim, M.-S.; Caron, F. Life cycle and management of carbon-14 from nuclear power generation. *Prog. Nucl. Energy* **2006**, *48* (1), 2−36.

(60) Elmquist, M.; Cornelissen, G.; Kukulska, Z.; Gustafsson, Ö. Distinct oxidative stabilities of char versus soot black carbon: Implications for quantification and environmental recalcitrance. *Global Biogeochem. Cycles* **2006**, *20* (2), GB2009.

(61) Hammes, K.; Schmidt, M. W. I.; Smernik, R. J.; Currie, L. A.; Ball, W. P.; Nguyen, T. H.; Louchouarn, P.; Houel, S.; Gustafsson, Ö.; Elmquist, M. Comparison of quantification methods to measure fire-derived (black-elemental) carbon in soils and sediments using reference materials from soil, water, sediment and the atmosphere. *Global Biogeochem. Cycles* **2007**, *21* (3), GB3016.

(62) Widory, D. Combustibles, fuels and their combustion products: A view through carbon isotopes. *Combust. Theory Modell.* **2006**, *10* (5), 831−841.

(63) Koch, D.; Bauer, S. E.; Del Genio, A.; Faluvegi, G.; McConnell, J. R.; Menon, S.; Miller, R. L.; Rind, D.; Ruedy, R.; Schmidt, G. A.; et al. Coupled aerosol-chemistry-climate twentieth-century transient model investigation: Trends in short-lived species and climate responses. *J. Clim.* **2011**, *24* (11), 2693−2714.

(64) Shindell, D.; Faluvegi, G. Climate response to regional radiative forcing during the twentieth century. *Nat. Geosci.* **2009**, *2* (4), 294−300.